Observations of the Directional Distribution of Ocean-Wave Energy in Fetch-Limited Conditions

L. H. HOLTHUIJSEN

Delft University of Technology, Delft, the Netherlands

(Manuscript received 12 March 1982, in final form 23 August 1982)

ABSTRACT

Directional energy distributions of wind-generated waves were observed with a relatively high directional resolution in fairly homogeneous and stationary wind fields in fetch-limited conditions using stereophotography of the sea surface. In a situation that is traditionally considered as the ideal fetch-limited wave-generation situation, the shapes of the observed distributions were found to agree well with the $\cos^{2s}(\theta/2)$ model proposed by Longuet-Higgins *et al.* (1963). In non-ideal situations in which the wind slanted across the upwind coastline or in which the upwind coastline was irregular, the shapes of the directional distributions were strongly influenced by the geometry of the upwind coastline. This suggests that the process of wave generation is directionally decoupled.

1. Introduction

The directional distribution of ocean-wave energy is an important parameter in many problems related to ocean waves. The considerable effort required to obtain detailed observations of this distribution has led to the use of model distributions which have been verified, if at all, with only a few such observations in the open ocean. The present study provides such a verification in fetch-limited conditions.

Among the models proposed in the literature to represent the directional energy distribution of ocean waves are the $\cos^2\theta$ model of Pierson *et al.* (1955) with a fixed directional width and the SWOP[1] model proposed by Coté *et al.* (1960) with a directional width depending on frequency and windspeed. Another model with a variable width is the $\cos^{2s}(\theta/2)$ model suggested by Longuet-Higgins *et al.* (1963). This model is being used on an increasingly wide scale and it has been chosen for comparison with the observations of this study. Tyler *et al.* (1974) concluded that this model was an adequate representation of their 10 high-resolution ($\sim 6°$) radar observations in duration-limited situations around Wake Island in the Pacific Ocean. Other, but rather indirect support for the $\cos^{2s}(\theta/2)$ model is provided by some buoy observations of Longuet-Higgins *et al.* (1963) and Mitsuyasu *et al.* (1975).

In the present study the directional energy distribution is determined as a function of wavenumber from stereophotographs of the sea surface in a manner similar to that used in the SWOP project (Coté *et al.*, 1960). The relatively high directional resolution of the observations (as compared to directional buoy observations) permits a quantification of the differences between model and observations. A simple parametric hindcast model is used to investigate the unexpectedly large influence of the geometry of the upwind coastline on the shape of the observed two-dimensional spectra.

A detailed description of the present study is given in the author's doctoral thesis (Holthuijsen, 1981).

2. Stereophotography of ocean waves

The application of stereophotography to the observation of ocean waves is a rather straightforward adaption of its conventional use in geodetic survey. The adaptions were implemented as early as 1904 in an experiment with cameras mounted on an ocean going ship (Schumacher, 1939). Later, airborne cameras were used in SWOP (Coté *et al.*, 1960) and several other studies (e.g. Simpson, 1967; Sugimori, 1975).

The major differences with the conventional use of stereophotography stem from the fact that the sea surface is a rapidly moving object. This requires that the pictures of a stereo photo pair be taken almost simultaneously. In fact, the maximum permissible time interval is typically 5 ms (Cruset, 1952; Coté *et al.*, 1960; Holthuijsen, 1981). This short time interval requires the use of two synchronized cameras. After a detailed investigation of a number of options, two radio-triggered Hasselblad 500 EL cameras with 50 mm lenses and 6 cm × 6 cm image format were used (Vliet, 1972). They were later replaced by two Jen-

[1] Stereo Wave Observation Project (Coté *et al.*, 1960).

optik UMK cameras with 100 mm lenses and 13 cm × 18 cm image format, when these came available (Vliet, 1974). The error of synchronization was ~0.2 ms for the system with the Hasselblad cameras and 3,0 ms for the system with the UMK cameras.

Each of the two cameras was mounted over a dropdoor in an Alouette III helicopter of the Royal Netherlands Air Force. The helicopters were flying side by side during the photographic operations, one helicopter maintaining a steady course with a specified speed, direction and altitude, the second helicopter maintaining a specified lateral distance to the leading helicopter. This distance was continuously estimated by an observer in the second helicopter who used the viewer of a third camera as a range finder. This camera was also used to determine the scale of the photography by measuring the distance between the cameras. It photographed the leading helicopter each time a stereo picture pair was taken. From the apparent size of the helicopter on the film the distance between the helicopters and thus between the cameras was calculated. It was approximately equal to half the altitude of photography which depended on the anticipated wave conditions. The choice of this altitude was a compromise between requirements related to spectral resolution and noise. For instance, to achieve a resolution of better than $0.1k_m$ and a noise-to-signal ratio of less than 0.1 (in terms of variances), the altitude for the system with the UMK cameras was chosen in the usually narrow window

$$10k_m^{-1} < h < 250H_s, \tag{1}$$

where k_m is the wavenumber at the peak of the spectrum and H_s is the significant wave height (Holthuijsen, 1981). For the observations reported here the altitude varied from 75 to 450 m. When the helicopters were flying in the required formation over the target area, the photographer started a photographic sequence by operating the radio transmitter. The sequence consisted usually of 10 stereo picture pairs of non-overlapping areas of the sea surface. The action of obtaining such a sequence was called a sortie.

The analysis of the stereopictures was conventional. An operator, scanning the three-dimensional image of the sea surface as it was reconstructed in a stereoscope, determined the sea surface elevation relative to an arbitrary plane of reference. This was done on a square grid in a Cartesian system of x, y and z coordinates of which the positive x and y axes were parallel to the camera main axes. As these were aligned with the main axes of the helicopters, the positive y axis pointed in the direction of flight. After this photogrammetric analysis the data were numerically prepared for the subsequent spectral analysis. This preparation consisted of clipping the areas of surface information to squares of equal size ($L \times L$) within each sortie and removing the two-dimensional linear trend from each of the squares with a least-squares method. A number of N, typically 10, spatial samples of the sea surface was thus obtained from each sortie.

3. Spectral analysis

The two-dimensional wavenumber spectrum $E(\mathbf{k})$ is defined as

$$E(\mathbf{k}) \equiv \int_0^\infty\int C(\mathbf{r}) \exp(-i2\pi\mathbf{k}\cdot\mathbf{r})d\mathbf{r}, \tag{2}$$

where $\mathbf{k}$ is the wavenumber vector and $C(\mathbf{r})$ the spatial covariance function of the sea surface elevation with $\mathbf{r}$ as the displacement vector. Note the factor 2π in this expression which makes the wavenumber equal to the reciprocal of a wavelength rather than the more conventional phase per unit distance. For each sortie this spectrum is estimated from the stereophotographic data by first computing the two-dimensional wavenumber spectrum of the sea surface elevation from each stereo picture pair with a multi-dimensional, multi-radix FFT procedure (Singleton, 1969). The spectral density is thus computed on a square grid in $\mathbf{k}$ space with grid-size $\Delta k_x = \Delta k_y = \Delta k = 1/L$ and with Nyquist wavenumbers $k_{a,x}$ and $k_{a,y}$ in the x and y directions, respectively. The average spectrum of the sortie is subsequently determined as the ensemble average of the individual spectra from the N square areas of sea surface information.

$$E(\mathbf{k}) = \frac{1}{N}\sum_{i=1}^{N} E_i(\mathbf{k}), \tag{3}$$

where $E_i(\mathbf{k})$ is the spectrum from the ith stereo picture pair and $E(\mathbf{k})$ is the final estimate of the two-dimensional wavenumber spectrum. It is transformed to the k, θ space with the straightforward transformation

$$E(k, \theta) = E(\mathbf{k})J, \tag{4}$$

where k and θ are the magnitude and the orientation of the wavenumber vector $\mathbf{k}$ and the transformation Jacobian J is equal to k. From this spectrum the directional energy distribution $D(\theta; k)$ is readily obtained as a function of wavenumber by scaling $E(k, \theta)$, i.e.,

$$D(\theta; k) = \frac{E(k, \theta)}{E(k)}, \tag{5}$$

where

$$E(k) = \int_0^{2\pi} E(k, \theta)d\theta. \tag{6}$$

As no tapering or filtering is used in the computation of $E(\mathbf{k})$, its spectral resolution (r_k in both k_x and k_y directions) would be approximately equal to the mesh-size in $\mathbf{k}$ space (Jenkins and Watts, 1968) if all pictures in a sortie were oriented in the same direction, i.e.,

$$r_k \approx \Delta k = 1/L. \tag{7}$$

The corresponding directional resolution (r_θ) in k, θ space, and hence the directional resolution of $D(\theta; k)$, would be approximately equal to 2π divided by the number of statistically independent estimates of $E(\mathbf{k})$ on a circle centered in $\mathbf{k} = \mathbf{0}$ with radius k:

$$r_\theta \approx \frac{\Delta k}{k}. \tag{8}$$

However, the orientation of the pictures is not constant during a sortie due to the yaw motion of the helicopters. It was established with independent photographic observations at sea (over a fixed platform) that the standard deviation of this motion (σ_{yaw}) is ~0.06 (~3.5°). The above estimate of the resolution is therefore adjusted by increasing it by twice the standard deviation σ_{yaw}:

$$r_\theta \approx \frac{\Delta k}{k} + 2\sigma_{yaw}. \tag{9}$$

The statistical reliability of the spectral estimates of $E(\mathbf{k})$, when expressed in the number of degrees of freedom of the χ^2-distribution is approximately $2N$ (Jenkins and Watts, 1968). This estimate of the reliability is not increased by the above reduction in resolving power because the number of independent spectral estimates in the ensemble average is not influenced by the variation in picture orientation.

4. Observations

From the 60 sorties flown for this study, four were selected as the most interesting with stereo pictures of acceptable quality. Two of these were observed in a geophysical situation which was fairly close to a situation in which a stationary, homogeneous wind blows over deep water, perpendicularly off a long and straight coastline. This is often considered to be the ideal generation situation in studies of wind–wave growth. Two other spectra were observed in situations differing from this ideal situation in that either the wind was slanting across the coastline or in that the upwind coastline was irregular. A label number and the overall characteristics of these situations are briefly indicated in Table 1.

TABLE 1. Overall geophysical characteristics of the observations.

Observation No.	Site	Distance off-shore (km)	Wind direction, wind speed	Coastline
1	Noordwijk	10.0	perpendicularly offshore, 6 m s^{-1}	long straight
2	Noordwijk	20.0		
3	Noordwijk	16.5	slanting, 10 m s^{-1}	
4	Sylt	46.2	perpendicularly offshore, 13 m s^{-1}	irregular

a. Site description

Three of the four spectra were observed off the coast of Holland in the southern North Sea near the town of Noordwijk (Fig. 1). This coast is long compared with the distance offshore of the observations and it is slightly concave when viewed from the sea (Fig. 3). The water is relatively deep for waves generated by an offshore wind of 25 m s^{-1} or less (Fig. 2). The fourth observation was taken off the coast of the island of Sylt in the southern North Sea in the framework of a continuation of JONSWAP (Hasselmann *et al.*, 1973). Before the analysis of the stereophotographic observations, the upwind coast (Fig. 5) was also considered to be long and straight (although slightly convex when seen from the sea) as only the coast of Sylt was deemed to be relevant to the observations. However, after the analysis it appeared that the upwind coast had to be considered on a larger scale. It is then quite irregular with the estuaries of the rivers Elbe and Weser to the south. The bottom profile off Sylt is similar to that off Noordwijk (Fig. 2) and the water is consequently deep water for the wind speeds indicated.

b. Meteorological conditions

The two observations in the ideal situation were carried out off Noordwijk on 12 November 1976 at approximately 1200 GMT. Synoptic information indicates that the meteorological situation was dominated by a stationary high pressure area (1015 mb) over the Norwegian Sea and a low pressure area (1000 mb) moving from the Bay of Biscay to northern France during the 12 h prior to the observations. The stereophotographic observations were made with an oceanographic observation tower in 10 km range and with three synoptic weather stations in a range of 70 km (Fig. 3). During the 12 h prior to the observations the 10 min average wind speed and wind direction at 10 m elevation decreased and backed slowly from ~9 m s^{-1} and 180° (nautical convention) to ~6 m s^{-1} and 140° at the time of the observations. In the last 2 h the variation in space and time, as observed at the weather stations, was less than 1 m s^{-1} and 20° from the latter values which were taken at the tower. This variation was deemed sufficiently small to consider the wind field as homogeneous and stationary on the scales relevant to the observations. As the wind direction of 140° is only 20° off the ideal offshore wind direction of 120°, the wind field was labeled as an ideal wind field.

The third observation was also carried out off Noordwijk, on 23 March 1976, at approximately 1100 GMT. A high pressure ridge, extending from the North Cape (1020 mb) to southern England (1010 mb) dominated the weather over the North Sea. This situation had persisted during the three days prior to the observations. The wind speed during the observations varied from a peak value of roughly 12 m s^{-1}

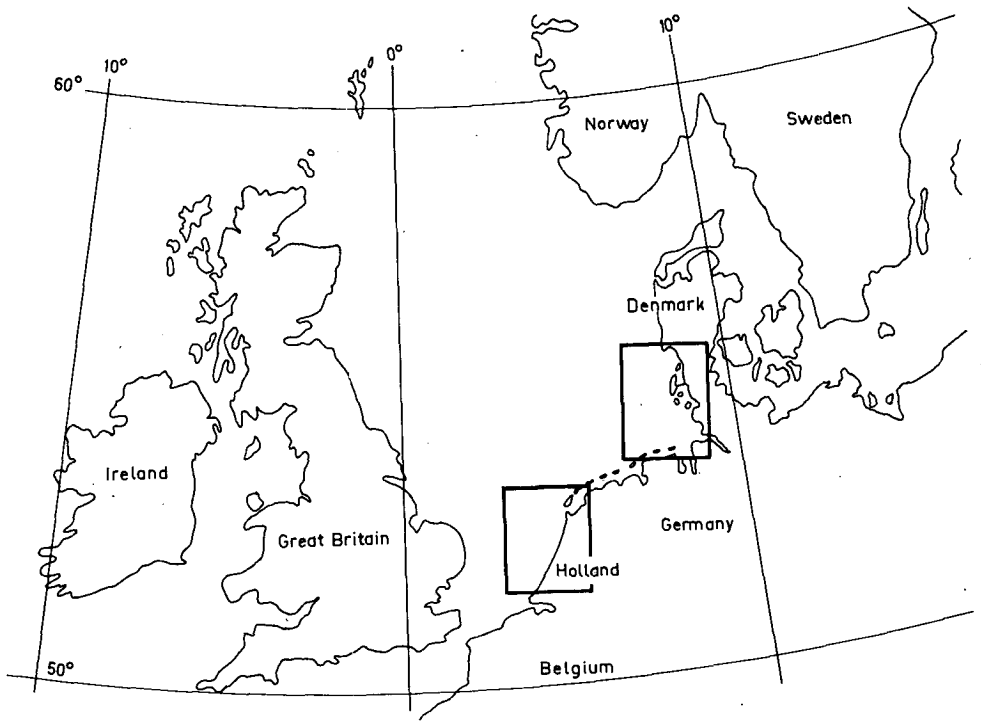

FIG. 1. The general geographic locations of the observations indicated by the boxes off the Dutch coast and off the German-Danish border. The areas in these boxes are enlarged in Figs. 3–5.

at 53° latitude to much lower values (<5 m s^{-1}) to the north and to the south. At the tower and at the two weather stations in the 180° upwind sector from the location of observation (at about 52°20′N latitude), the wind speed and wind direction were fairly constant at ~10 m s^{-1} and 70° (Fig. 4). This is a direction ~50° backed with respect to the ideal offshore wind direction. During the last 12 h prior to the observations, the variation in time and space in this sector, as observed at the weather stations, was less than 2 m s^{-1} for the wind speed from the stated value while the wind directions at the weather stations were slightly veered (20–30°) with respect to the wind direction at the tower (70°) but otherwise fairly stationary with a maximum deviation at each station of about 10° from the 12 h mean value. These observed variations were considered sufficiently small to label the generating wind field as fairly homogeneous and stationary on the scales relevant to the observations (up to 53°N). In the 180° downwind sector the wind speed was much lower than in the upwind sector, but as waves are mostly generated in the upwind sector, this decrease of wind speed downwind does not influence the assessment of the generating wind field.

The fourth observation was obtained off Sylt on 18 September 1973 at 1630 GMT, again in a wind field which was considered to be fairly homogeneous and stationary. The weather was dominated by a frontal system just west of the area of observation between a depression (1000 mb) over the Irish Sea and a region of high pressure (1025 mb) over the Baltic Sea. This system moved slowly eastwards with the frontal passage some hours after the observations. In the area

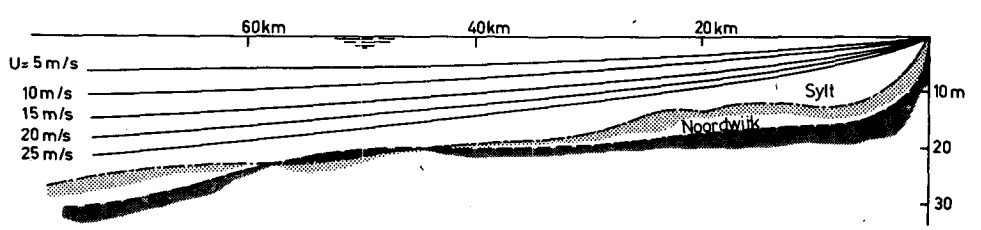

FIG. 2. Bottom profiles normal to the coast off Noordwijk and Sylt. The depth at the drawn lines is one-quarter of the wavelength corresponding to the peak frequency of the spectrum generated by an offshore wind with the indicated wind speed (Hasselmann *et al.*, 1973).

of observation one weather station was available (Fig. 5). The wind speed and wind direction there were rather stationary at 13 m s^{-1} and 115° for a period of more than 12 h prior to the observations, the observed temporal variations being less than 1 m s^{-1} and 10° from these mean values (Brümmer *et al.*, 1974). This wind direction is only 8° off the ideal offshore wind direction of 107° (Hasselmann *et al.*, 1973). Such a stationary situation in a moving atmospheric system suggests a fairly homogeneous wind field. This is roughly supported by synoptical information but the scale of the weather maps does not permit a detailed analysis of the local situation.

c. *Stereophotographic observations*

The photographic and photogrammetric procedures provided the sea surface elevation as a function of horizontal coordinates in approximately 10 non-overlapping squares of sea surface areas per sortie. The most relevant parameters for the photographic operations and the photogrammetric analysis have been addressed earlier. Their values are listed in Table 2. The mesh size, related to the Nyquist wavenumbers

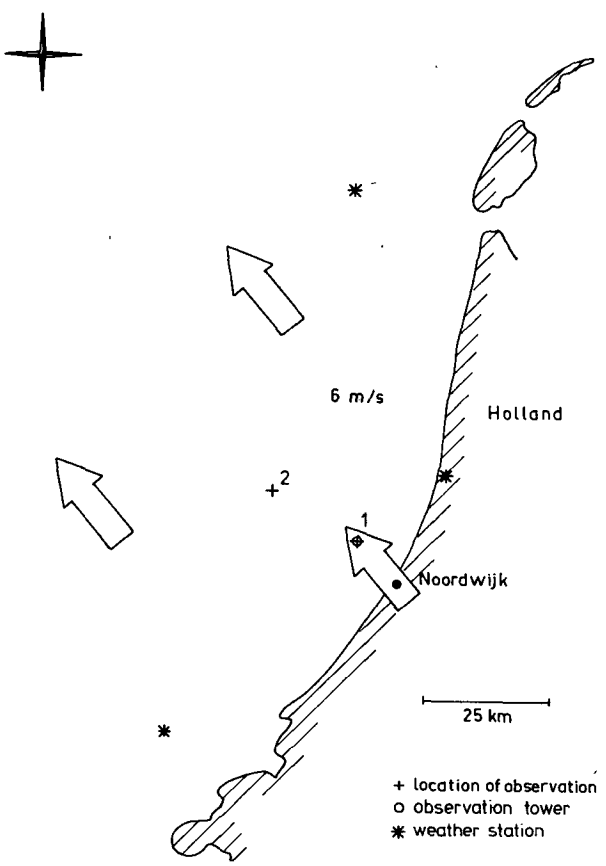

FIG. 3. The ideal generation situation of observations 1 and 2 with a constant wind blowing over relatively deep water almost perpendicularly off a long and straight coastline.

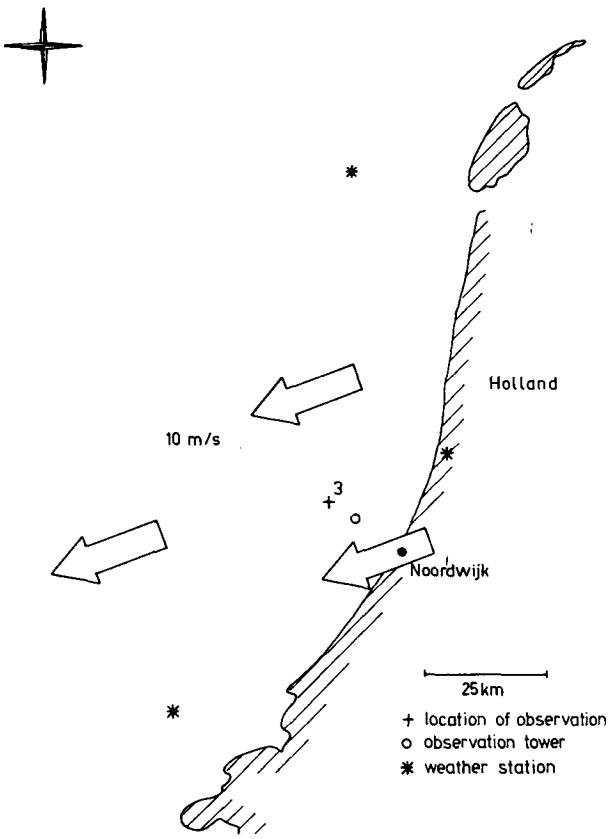

FIG. 4. The slanting-wind situation of observation 3 with a constant wind blowing over relatively deep water off a long and straight coast line from a direction which is 50° off the normal to the coast.

$k_{a,x}$ and $k_{a,y}$, was chosen so as to have only a few percent of the anticipated total wave energy aliased. The direction of the y axis is equal to the direction of the main helicopter axis during the observations. It should be noted that two of the stereo areas in observation 1 overlapped each other for 40% in surface area. The number of degrees of freedom for this observation is reduced proportionally but the directional resolution is hardly affected.

d. *Observed spectra and directional distributions*

The two-dimensional wavenumber spectra obtained with the spectral analysis of the photogrammetric observations are presented in Fig. 6 as contoured plots of the energy density. These contour lines are rather jagged, which is mainly due to the statistical variation of the spectral estimates. More intelligible versions of these original plots are given later in a discussion of these spectra. Some relevant parameters of the observations are given in Table 3. The directional distributions $D(\theta; k)$ taken from the observed spectra $E(k, \theta)$ are statistically almost independent of each other as they were taken at an interval Δk along the k axis. The four observed spectra thus provided

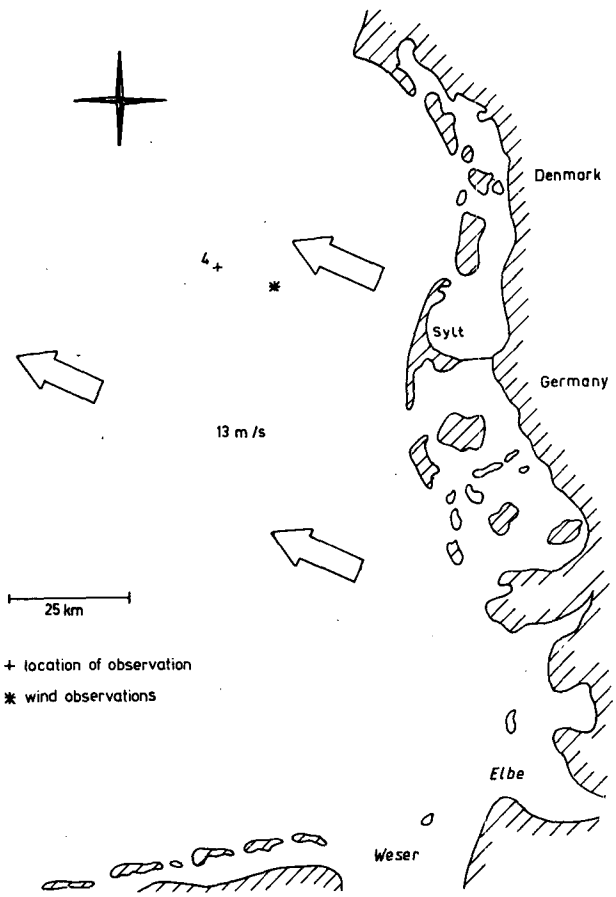

FIG. 5. The irregular coast situation of observation 4 with a constant wind blowing over relatively deep water off a long and irregular coastline.

a total of 74 independent distributions, 28 in the "ideal" generation situation and 46 in the non-ideal situation. As representative samples from this set of observations, those at the peak wavenumber and at twice the peak wavenumber are illustrated in Fig. 7.

5. Model fitting

a. Model distribution

The $\cos^{2s}(\theta/2)$ model, indicated by $D^*(\theta)$ in the following, has two free parameters per wavenumber: the mean direction $\bar{\theta}$ and the directional width parameter s:

$$D^*(\theta) = A_1 \cos^{2s}[(\theta - \bar{\theta})/2], \tag{10}$$

where

$$A_1 = \frac{1}{2\pi^{1/2}} \frac{\Gamma(s+1)}{\Gamma(s+\frac{1}{2})}$$

is a normalization coefficient. Unfortunately the directional width parameter s is not expressed in terms of a directional sector (such as, e.g., the directional standard deviation of a circular normal distribution) nor is it a linear indicator of the width in terms of such a sector. Such information is considered appropriate here and the directional width is thus also, but only for illustrative purposes, expressed in the directional standard deviation

$$\sigma_\theta = \left[\int_{-\pi}^{+\pi} \theta^2 A_1 \cos^{2s}(\theta/2) d\theta\right]^{1/2}. \tag{11}$$

The relationship between σ_θ and s is

$$\sigma_\theta \approx [2/(s+1)]^{1/2} \tag{12}$$

for $\sigma_\theta < 60°$, say (the approximation is that $\theta \simeq 2 \times \sin(\theta/2)$).

To account for the 180° ambiguity inherent in photographic observations, the model $\hat{D}(\theta)$ which was actually fitted to the observations was a modified version of the $\cos^{2s}(\theta/2)$ model:

$$\hat{D}(\theta) = \tfrac{1}{2}[D^*(\theta) + D^*(\theta + \pi)]. \tag{13}$$

b. Parameter estimation

Prior to the shape analysis the observations were filtered to some extent. Two aspects were considered. The first is the presence of locally excessive noise (in the **k** plane). An inspection of the contoured plots of the observed spectra (Fig. 6) reveals that these spectra have a relatively high density near the k_x axis and also near the k_y axis in observation 1. Along the k_x axis this noise is related to the scanning procedure of the photogrammetric analysis in which a low-amplitude saw-tooth wave is inadvertedly superimposed on the surface with a wavelength of $2\Delta x$ and a crest direction along the y axis. A stereophotogrammetric analysis of mechanically generated regular waves in a hydraulic laboratory showed that the estimate of the surface elevation along one scan direction is generally slightly too low whereas it is slightly too high along the opposite scan direction. The shape of the resulting saw-tooth wave agrees with the one observed: a sharp peak at the Nyquist wavenumber $k_{a,x}$ and a ridge along the k_x axis. The ridge along the k_y axis in observation 1 may have been generated in a similar manner if the direction of scanning was changed in only a few pictures of this sortie from parallel to the y axis to parallel to the x axis. These

TABLE 2. Main characteristics of the photographic sorties and of the photographic analysis.

Observation No.	Altitude (m)	Direction of y axis (°T)	Side of square area (m)	Side of square mesh (m)	Number of areas
1	75	275	54.0	1.5	8
2	150	275	156.0	3.0	10
3	150	310	170.0	2.5	9
4	450	110	220.0	5.0	9

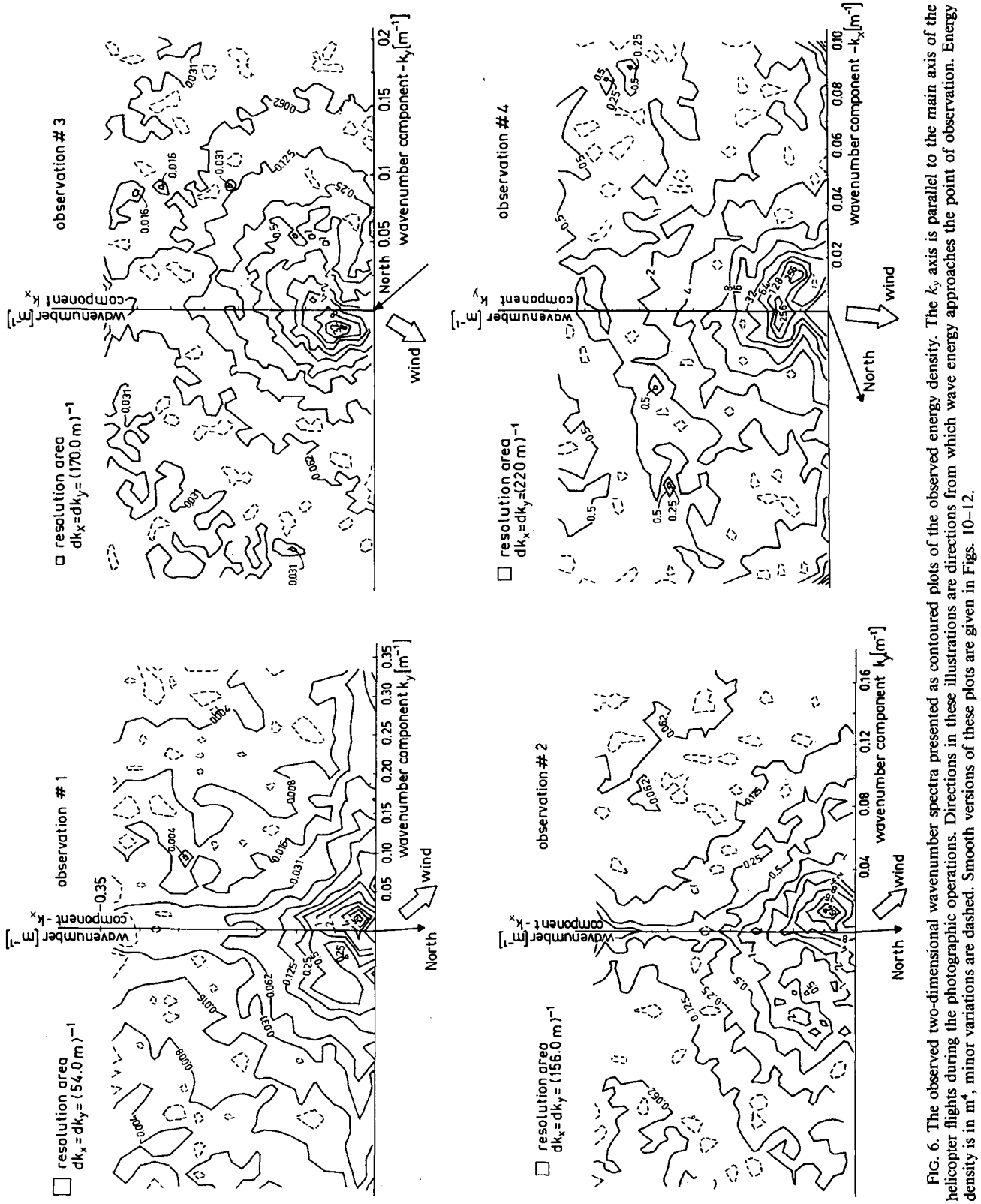

FIG. 6. The observed two-dimensional wavenumber spectra presented as contoured plots of the observed energy density. The k_y axis is parallel to the main axis of the helicopter flights during the photographic operations. Directions in these illustrations are directions from which wave energy approaches the point of observation. Energy density is in m^4, minor variations are dashed. Smooth versions of these plots are given in Figs. 10–12.

TABLE 3. Statistical reliability, peak wavenumber, peak wavelength and directional resolution of the observed wavenumber spectra.

Observation No.	Degrees of freedom per spectral estimate	Peak* wavenumber k_m (m^{-1})	Peak wavelength k_m^{-1} (m)	Directional resolution at (deg)	
				$k = k_m$	and $k = 2k_m$
1	15	0.0926	10.8	18	13
2	20	0.0641	15.6	13	10
3	18	0.0263	38.0	19	13
4	18	0.0187	53.5	21	14

* Local sea.

areas with noise, where the contour lines were persistently more or less parallel to the k_x or k_y axes, were subsequently ignored in the shape analysis. So was an area near $\mathbf{k} = \mathbf{O}$ in observation 4 which was influenced by a dome-shaped distortion of the sea surface in the stereo pictures of this observation. In observations 1 and 2 swell was present from a direction 220° (reference is made to the discussion in Section 7a). It was ignored in the shape analysis as this study is concerned only with locally generated seas. The method by which the $\cos^{2s}(\theta/2)$ model is fitted to each of the observed directional distributions, indicated by $\tilde{D}(\theta)$, is a least-squares method in which the mean-square difference,

$$V_1 = \int_0^{2\pi} [\tilde{D}(\theta) - \hat{D}(\theta)]^2 d\theta, \qquad (14)$$

is minimized while varying the model parameters $\bar{\theta}$ and s simultaneously.

c. *Goodness of fit*

The value of the mean square difference V_1 is a convenient measure of the difference between model and observation. A normalized version has been used by Tyler *et al.* (1974):

$$V_2 = \frac{\int_0^{2\pi} [\tilde{D}(\theta) - \hat{D}(\theta)]^2 d\theta}{\int_0^{2\pi} [\tilde{D}(\theta)]^2 d\theta}. \qquad (15)$$

However, to avoid the individual evaluation of each of a large number of values of V_2 (one for each wavenumber), an integral version was chosen to represent the observed differences for each spectrum as a whole, i.e.,

$$V_3 = \frac{\int_0^{\infty}\int_0^{2\pi} \tilde{E}(k)^2[\tilde{D}(\theta) - \hat{D}(\theta)]^2 d\theta dk}{\int_0^{\infty}\int_0^{2\pi} \tilde{E}(k)^2[\tilde{D}(\theta)]^2 d\theta dk}, \qquad (16)$$

where $\tilde{E}(k)$ is the observed one-dimensional wavenumber spectrum. The residuals are weighted here with the one-dimensional energy density to allow for the fact that the differences between the observation and the model are deemed to be more important in the energetic part of the spectrum than in other parts. Note that V_3 may also be written as

$$V_3 = \frac{\int_0^{\infty}\int_0^{2\pi} [\tilde{E}(k, \theta) - \hat{E}(k, \theta)]^2 d\theta dk}{\int_0^{\infty}\int_0^{2\pi} [\tilde{E}(k, \theta)]^2 d\theta dk}, \qquad (17)$$

where $\tilde{E}(k, \theta) = \tilde{E}(k)\tilde{D}(\theta)$ and $\hat{E}(k, \theta) = \tilde{E}(\theta)\hat{D}(\theta)$. Although the value of $V_3^{1/2}$ provides a quantitative overall measure of the differences between observation and model, it does not indicate to what extent the statistical variability of the observation is responsible for these differences. This is investigated with the

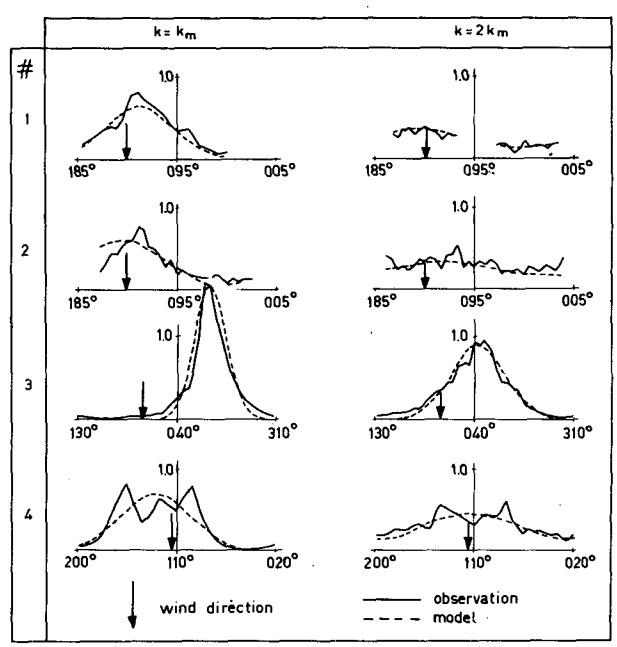

FIG. 7. The observed directional wave-energy distributions at the peak wavenumber k_m and at twice the peak wavenumber $2k_m$ as representative samples of the 74 observed directional distributions and the corresponding least-squares fits of the $\cos^{2s}(\theta/2)$ model. The directional resolution of the distributions varies between 10 and 20° (see Table 3). Swell and noise have been omitted.

notion of sample variability in the following Monte-Carlo technique.

Given the geophysical and statistical conditions of the observation of one of the observed spectra in this study, one can conceive of a large set of spectra which could be obtained under identical conditions. If a sufficiently large number of such spectra is considered, this set constitutes a population of observable spectra, each of which differs from each of the others in this set because of the random nature of the observations. The spectrum actually observed in the present study will be compared with two types of spectra. One is a randomly selected spectrum $\tilde{E}'(k, \theta)$ from the above population of observable spectra and the other is the model spectrum $\hat{E}(k, \theta)$. If the difference between the actually observed spectrum and the model spectrum is smaller than the difference between this actually observed spectrum and the randomly selected spectrum, the model is said to be statistically consistent with the observation. In more quantitative terms, we define the difference between the actually observed spectrum $\tilde{E}(k, \theta)$ and a sample spectrum $\tilde{E}'(k, \theta)$ as

$$V_4' = \frac{\int_0^\infty \int_0^{2\pi} [\tilde{E}(k, \theta) - \tilde{E}'(k, \theta)]^2 dk d\theta}{\int_0^\infty \int_0^{2\pi} [\tilde{E}(k, \theta)]^2 dk d\theta}. \quad (18)$$

Since the sample spectrum $\tilde{E}'(k, \theta)$ is a random variable, the difference V_4' is a random variable. Its probability density function is denoted as $p(V_4)$ and its α-fractile value $V_{4,\alpha}$ is defined by

$$\alpha = \int_{V_{4,\alpha}}^\infty p(V_4) dV_4. \quad (19)$$

If the difference V_3 between the actually observed spectrum and the model spectrum is smaller than $V_{4,\alpha}$, the $\cos^{2s}(\theta/2)$ model is said to be statistically consistent with the observation at the α-level of confidence.

To establish the statistical consistency of the model with one of the observations of this study, the probability density function $p(V_4)$ is estimated here by first generating numerically a large set of sample spectra corresponding to the one chosen observation and by then determining V_4' for each of these sample spectra. These values of V_4' are ordered in a histogram from which $V_{4,\alpha}$ is estimated. Each of the sample spectra is estimated as follows. As indicated in Section 3, the spectral densities at the grid-points in the **k** plane are independently χ^2 distributed with $2N$ degrees of freedom each. If the expected value of this χ^2 distribution is taken to be the actually observed spectral density, then both parameters of the χ^2 distribution are available at each grid-point and one number is randomly drawn from this distribution at each grid-point. This set of numbers constitutes a new spectrum which is a sample observable spectrum in **k** space corresponding to the chosen observed spectrum. Transforming this spectrum to k, θ space along the lines described in Section 3 provides a sample observable spectrum $\tilde{E}'(k, \theta)$ whose value of V_4' is readily determined. This process of drawing a sample observable spectrum in **k** space from the above population, then transforming it to k, θ space and determining its value of V_4' is repeated a few hundred times, resulting in a histogram of V_4' and an estimate of $V_{4,\alpha}$ for the chosen observed spectrum.

6. Observed directional parameters and goodness of fit

The values of the directional parameters $\bar{\theta}$ and s which were found from the least-squares fit of the $\cos^{2s}(\theta/2)$ model to the observed distributions are given in Fig. 8. The goodness of fit, as quantified by the values of the normalized root mean square differences $V_3^{1/2}$ of the residuals is given in Table 4 for each spectrum. Illustrations of the goodness of fit are given for a few representative observations in Fig. 7. The influence of sample variability on the difference between observation and model is investigated for observation 1 only (for reasons of economy). This spectrum is chosen mainly because it was generated in the "ideal" generation situation. It was preferred over the spectrum of observation 2, which was also generated in this situation, as it has the smallest number of independent directional distributions of the two spectra (again a reason of economy). A total of 500 sample spectra is drawn and the histogram of the 500 corresponding values of V_4' is given in Fig. 9. The values of V_3 (=0.040) and $V_{4,0.05}$ (=0.308) are also indicated.

7. Discussion

The discussion of the results will pertain to three aspects of the observations. The first is the overall shape of the two-dimensional spectra, in particular how it is influenced by the geometry of the upwind coastline. The second is the correspondence between the observed directional distributions and the $\cos^{2s}(\theta/2)$ model. The third aspect is the relationship between the directional width parameter s on the one hand and wind speed and frequency on the other.

a. Two-dimensional spectra

In the discussion of the observed two-dimensional wavenumber spectra, reference will be made to illustrations of these spectra. The contoured plots presented in Fig. 6 show fine detail which to some degree is due to the statistical variability of the observations. This is not relevant for an interpretation in physical terms, and smoother contoured plots (e.g., Fig. 10)

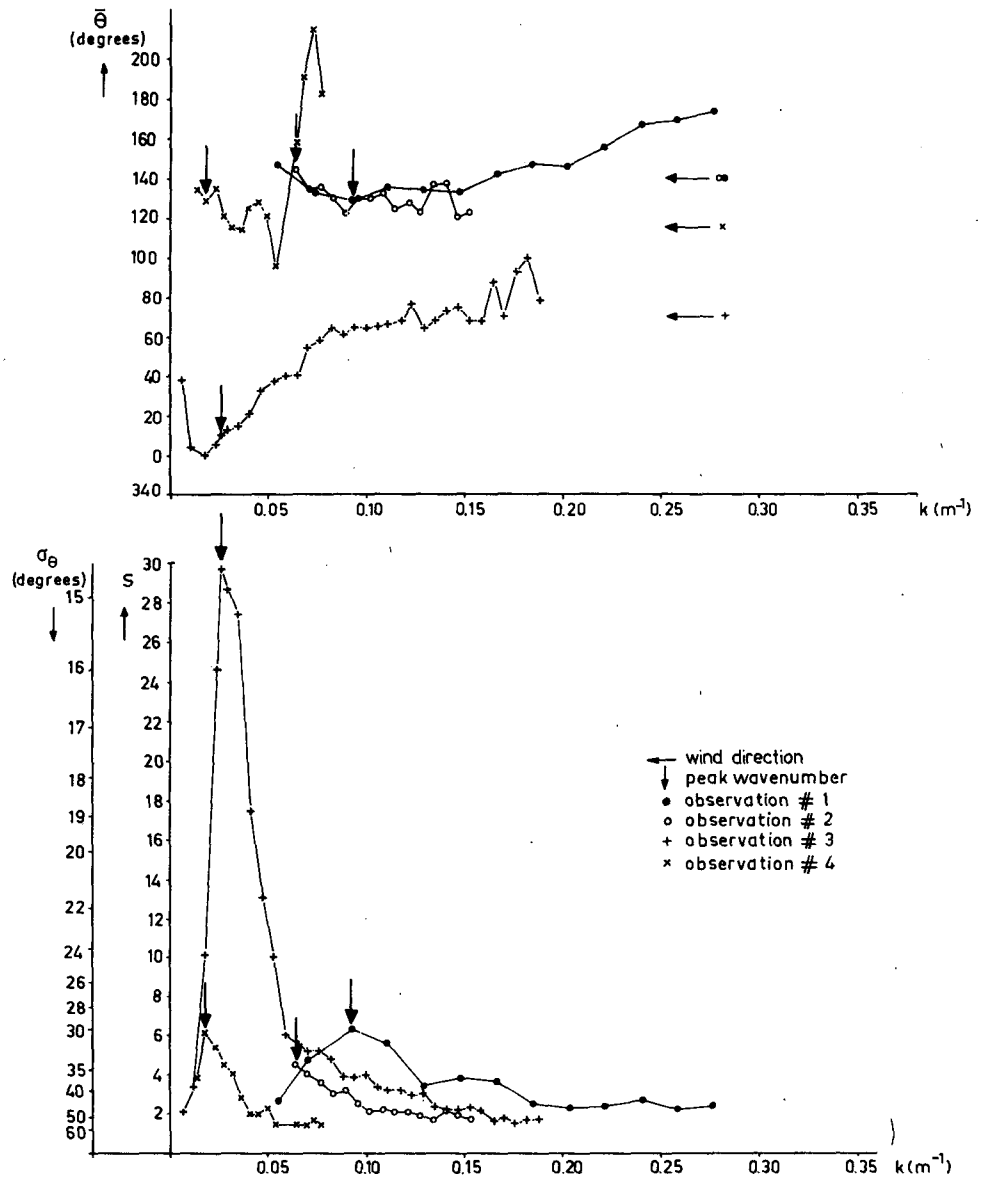

FIG. 8. The observed values of the main wave direction $\bar{\theta}$ and of the directional width parameter s of the $\cos^{2s}(\theta/2)$ model as function of wavenumber (inverse wavelength). The circular standard deviation σ_θ is the directional width of the $\cos^{2s}(\theta/2)$ model in terms of a directional sector. Swell and noise have been omitted.

are presented in which the original contour lines are hand-smoothed to emphasize the main features of the observed spectra.

1) THE IDEAL GENERATION SITUATION

The smoothed contour lines of observations 1 and 2 off the Dutch coast are given in Fig. 10 together with an indication of the generation conditions.

These spectra have essentially two peaks: one well-defined peak from the direction of 220° (waves coming from that direction) and another approximately from the wind direction, not so well defined since it is much broader and has secondary maxima.

The sharp peak at 220° represents waves which were probably generated in an area somewhere to the

TABLE 4. Goodness-of-fit between model and observation and number of observed distributions.

Observation No.	$V_3^{1/2}$	Observation No.	$V_3^{1/2}$
1	0.20	3	0.23
2	0.25	4	0.34

southwest of the area of observation. However, it is not possible with stereophotography to discriminate wave components traveling in opposite directions so that from these spectra alone one may as well conclude that these waves were generated in an area to the northeast of the area of observation. This is physically possible since both directions (220° and 40°) are more or less parallel to the coast. But a close inspection of detailed weather maps suggests that these wave components were generated in an atmospheric disturbance near the Strait of Dover (located in the direction 230°). The other peak in these spectra corresponds obviously to the locally generated wind sea. The two peaks are well separated both in direction and wave-number and the separation between the two wavefields was taken to be the line of steepest descent (estimated subjectively) from the saddle point between the two peaks.

Inspection of the wind-sea region in these spectra shows that the directional distributions are practically uni-modal and that the directional width is smallest near the spectral peak. This is in general agreement with other observations in the literature (e.g., Mitsuyasu *et al.*, 1975). A quantitative discussion of the directional width will be given later.

2) THE SLANTING WIND SITUATION

The smoothed contour lines of the spectrum observed in the slanting wind situation are given in Fig. 11, again with the generation conditions.

This spectrum has one rather pronounced peak from ~15° which is a direction more or less parallel to the coast. This is, at first sight, a surprising observation since the wind was blowing across the coastline from a direction of 70°. The wave components from northerly directions apparently dominated the wave components generated around the wind direction near the peak. For higher wavenumbers this dominance disappears as the main directions are closely aligned with the wind direction. As in observations 1 and 2, the directional distributions are practically uni-modal and most narrow near the peak.

The fact that wave components from the north dominated the wave components generated around the wind direction suggests that wave components from different directions are generated independently from each other. This aspect of wave generation will be addressed later in this section.

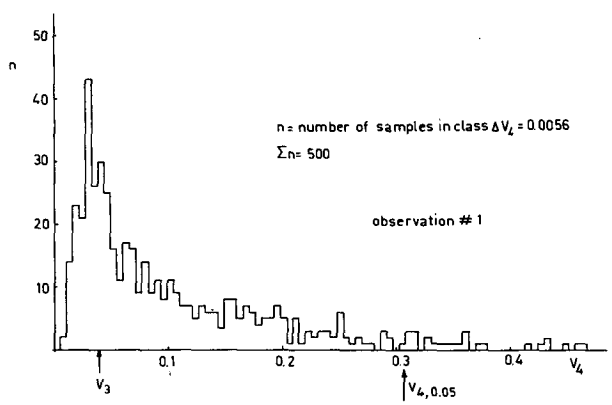

FIG. 9. The histogram of the numerically generated values of V_4' to quantify the influence of sample variability on the observed differences between the observations and the $\cos^{2s}(\theta/2)$ model for the ideal generation situation. V_3 is the actually observed difference.

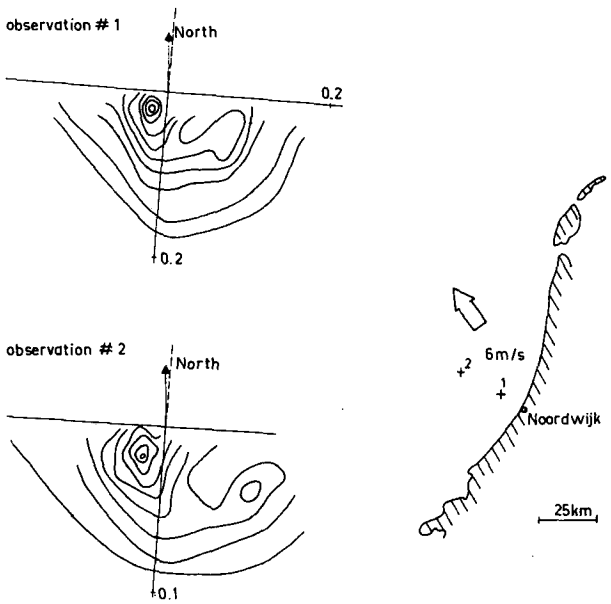

FIG. 10. For observations 1 and 2 in the ideal generation situation, the smoothed contour lines of the observed spectra (from Fig. 6) and the generation conditions (from Fig. 3). The axes in the k plane are 5° off the east–west or north–south directions. The peak in the lower right-hand quadrant represents locally generated waves, the sharp peak in the lower left-hand quadrant is swell generated near the Strait of Dover.

3) THE IRREGULAR COAST SITUATION

The smoothed contour lines of the spectrum of observation 4 and the generation conditions are given in Fig. 12. This spectrum has essentially two peaks: one from the wind direction and one from a direction which is 45° veered with respect to the wind direction. As the wind direction was south to southeast over the entire North Sea and Norwegian Sea, it seems obvious that the latter peak corresponds to wave components generated in the area south of Sylt with the deep indentations of the Elbe and Weser estuaries. This suggests also, as in observation 3, a directionally decoupled generation of waves.

The peak in the direction of the wind is bi-model (Fig. 7): two peaks can be identified differing approximately +15° and −15° in direction from the

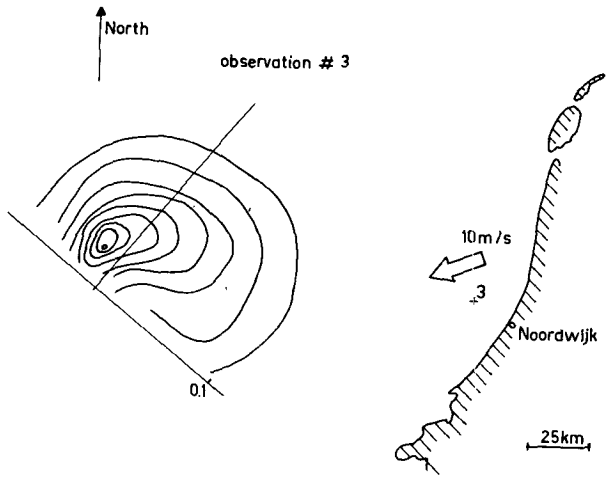

FIG. 11. For observation 3 in the slanting fetch situation, the smoothed contour lines of the observed spectrum (from Fig. 6) and the generation conditions (from Fig. 4). The axes in the **k** plane are 50° off the east-west or north-south directions. The waves at the peak of the spectrum travel more or less from the north parallel to the coast although they are generated by the offshore wind.

wind direction. It is noted also that some of the observations of Tyler *et al.* (1974) show bi-modality near the peak of the directional distribution. However, it is not observed in the other spectra of the present study. Whether this bi-modality is related to processes of wave generation such as for instance the nonlinear interactions in the bi-modal low-frequency lobe of the interaction function computed by Fox (1976) has not been investigated.

4) DIRECTIONALLY DECOUPLED WAVE GENERATION

The contribution of nonlinear resonant wave–wave interactions to the generation of wind waves is considerable, not only because they are to a great extent responsible for the shift of the peak frequency to continuously lower frequencies (presumably with a low-frequency limit), but also because they tend to stabilize the shape of the spectrum. This stabilizing effect seems to be present not only in ideal wave-generation situations but also in variable wind fields over the ocean (in generating conditions). Results of computations and observations have demonstrated this quite convincingly for the frequency spectrum (e.g., Hasselmann *et al.*, 1973, 1976). However, the effect of the nonlinear interactions on the shape of the directional energy distribution is very much open to discussion as long as similar computations and observations are not available in the f, θ domain. The practical implications (e.g. in wave forecasting) of the nonlinear interactions for the directional characteristics of waves are therefore still uncertain although Hasselmann *et al.* (1976) argue that for all practical purposes in wave forecasting the directional energy distribution conforms to a universal shape.

The shape of the two spectra observed in this study in non-ideal conditions indicate that the nonlinear interactions had not forced the spectral shape into a universal form. This suggests that the main directional characteristics of the observed spectra can be hindcasted with a model in which the nonlinear interactions between wave components from different directions are ignored. A model based on such a directional decoupling has been suggested by Seymour (1977). The essential characteristics are described as follows. Consider a stationary, homogeneous wind field with an arbitrary geometry of the upwind coastline (Fig. 13). Wave components coming from a direction θ_0 off the wind direction are treated as having been generated independently from wave components propagating in other directions. This implies that for the components from direction θ_0 only the wind speed U and the distance l in the direction θ_0 to the upwind coastline are relevant parameters. All other information on the geometry of the coastline is irrelevant for these components. It follows that the spectrum in the direction θ_0 is identical to the spectrum in that direction in arbitrarily different situations as long as the wind speed and the value of l are the same. The most obvious choice of such a situation, where the spectrum is relatively well documented, is the ideal wave-generation situation with a fetch equal to $l\cos\theta$. In the present study the JONSWAP spectrum is chosen with a $\cos^{2s}(\theta/2)$ directional distribution. The parameters of this two-dimensional spectrum were taken from Günther *et al.* (1979) and Hasselmann *et al.* (1980), with some modifications to avoid unexpected overshoot phenomena

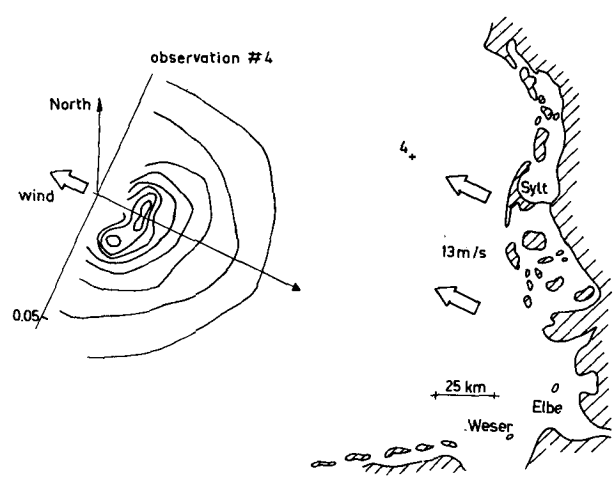

FIG. 12. For observation 4 in the irregular coast situation, the smoothed contour lines of the observed spectrum (from Fig. 6) and the generation conditions (from Fig. 5). The axes in the **k** plane are 20° off the east–west or the north–south directions. The two peaks represent waves generated by the offshore wind off Sylt and, independently, off the Elbe and Weser estuaries.

in the transition from a young sea state to the fully developed sea state and also to avoid side lobes in the two-dimensional spectrum in the fully developed situation (Holthuijsen, 1981).

The result of the hindcast in the irregular-coast situation off Sylt is indicated in Fig. 14 with the contour lines at the levels of 5% and 50% of the hindcasted maximum energy density. The observed peaks are also indicated. The hindcasted directions of the peaks, and to some extent the directional width of these peaks, agree even quantitatively well with the observations. This agreement is taken as an indication that the waves generated off Sylt did not interact appreciably with the waves generated off the coastal indentations south of Sylt.

A similar influence of the geometry of the upwind coastline on the shape of the two-dimensional spectrum is found in the slanting wind situation. The result of this hindcast is shown in Fig. 15. It should be noted that the weakening of the wind field to the north was represented in the model by introducing a coastline on the 53°N parallel. The main point in the comparison between observation and hindcast here is the shift of the main wave direction from parallel to the coast at low frequencies to the wind direction at high frequencies. In the illustrations the main direction of the observed spectrum is $\bar{\theta}$ resulting from the least-squares fit of the $\cos^{2s}(\theta/2)$ model to the observations, whereas the main direction of the hindcasted spectra is taken from the zeroth and first moment of the hindcasted directional distribution.

The observed and hindcasted shift can be understood as follows. The main wave directions for the low frequencies are northerly because these frequencies are mainly generated in fetches which are longest in northerly directions. This dominance diminishes gradually for increasing frequency because these frequencies increasingly approach the saturated stage where fetch considerations are irrelevant and where the main wave direction is equal to the wind direction. The qualitative agreement between observation and hindcast again suggests that the main directional

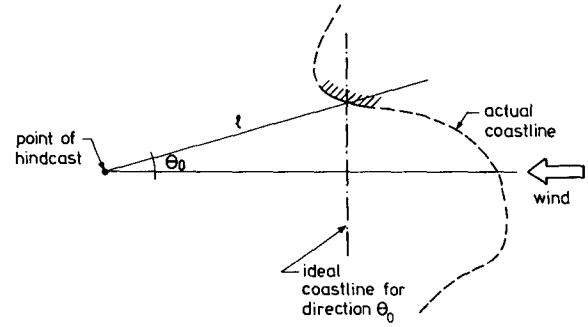

FIG. 13. Definition of the geometric parameters for the hindcast model in which the process of wave generation is directionally decoupled.

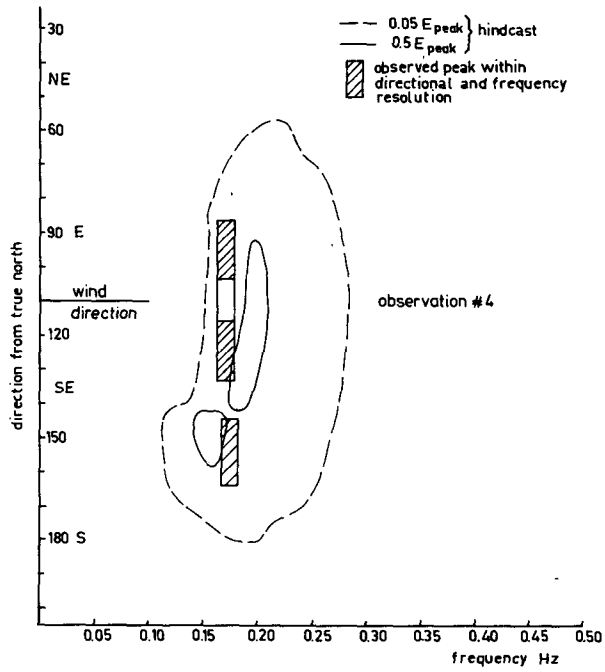

FIG. 14. The observed and hindcasted location of the two peaks in the f, θ plane in the irregular-coast situation. The observed and hindcasted peaks near 160° correspond to waves generated off the Elbe and Weser estuaries whereas the rather broad observed and hindcasted peaks near the wind direction of 110° correspond to waves generated off Sylt.

characteristics of the spectrum can be hindcasted under the assumption of directionally decoupled wave generation.

b. *The directional distribution*

The differences between the observed directional distribution and the $\cos^{2s}(\theta/2)$ model as quantified in the normalized root-mean-square difference $V_3^{1/2}$ (Table 4) cannot be assessed in an absolute sense because an appreciation of these numbers depends to a large extent on the purpose of modelling the spectrum. However, it is felt (rather subjectively) that the $\cos^{2s}(\theta/2)$ model describes the observations adequately for most purposes in the ideal wave-generation situation, particularly since the results of the consistency test indicate that the model is statistically consistent with the observed distributions in observation number 1 at the usually chosen 5% level of confidence (Fig. 9). In fact, the observed difference between the observation and the model ($V_3 = 0.040$) is almost equal to the most probable difference ($V_4 = 0.031$) between the observation and a hypothetically repeated observation. A quantitative comparison of the goodness of fit for the observations in the ideal generation situation with information from the literature is possible for the observations of Tyler *et al.* (1974). These authors determined the normalized

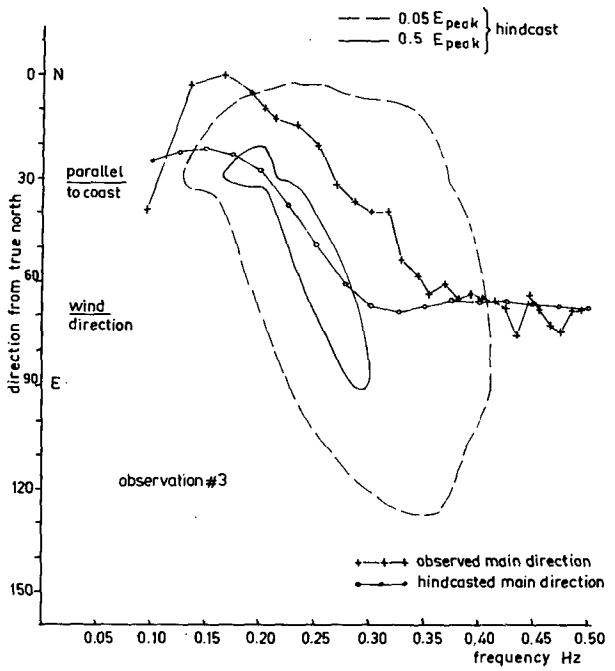

FIG. 15. The observed and hindcasted tendency of the main wave direction to shift from almost north at low frequencies to parallel with the wind direction at high frequencies in the slanting-wind situation. The lower frequencies are fetch-dominated which results in the observed and hindcasted main wave direction from almost north. The high frequencies are fully developed and the main wave direction is equal to the wind direction.

difference V_2 between a $[\cos^{2s}(\theta/2) + \alpha_0]$ model and each of 10 very detailed (directional resolution $r_\theta \simeq 6°$) radar observations of the directional distribution in a slowly varying wind field around Wake Island in the Pacific Ocean. The value of $V_2^{1/2}$ for each observed distribution individually (the linear fit in their Table 1) varied from 0.10 to 0.26 with an average value of 0.17. This is a slightly better fit than found in this study ($V_3^{1/2} = 0.20$ and 0.25), possibly because the model used by Tyler *et al.* has one more degree of freedom (in the uniform background α_0) than the model used in this study.

The directional distributions in the slanting-wind situation and in the irregular-coast situation are too much influenced by the geometry of the upwind coastline to expect a universal model distribution to be applicable. However, in the slanting-wind situation the $\cos^{2s}(\theta/2)$ model is still acceptable ($V_3^{1/2} = 0.23$) but the main direction $\bar{\theta}$ deviates considerably from the wind direction.

c. *The directional width*

The observed values of s in the present study can be compared with suggestions in the literature from Mitsuyasu *et al.* (1975) and Hasselmann *et al.* (1980). It appears from these suggestions that the value of s depends on the peak frequency and the wave age (to be defined later). The expressions will not be given

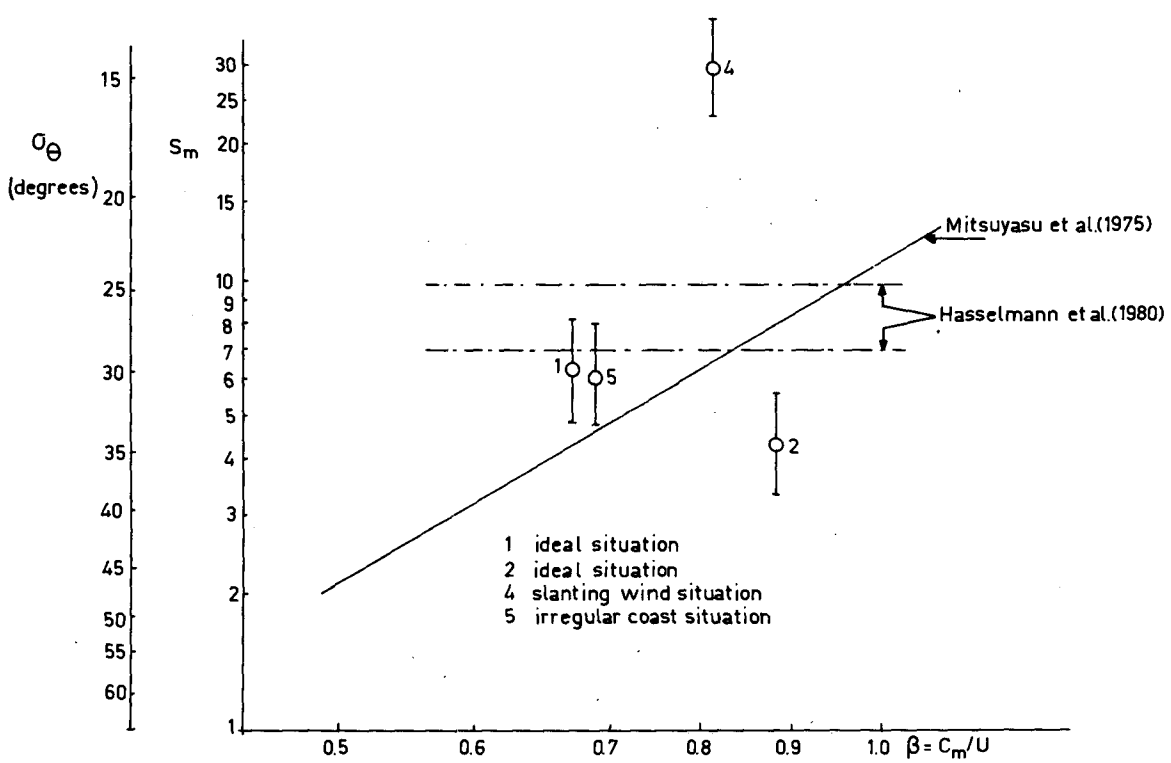

FIG. 16. The observed directional width parameter $s = s_m$ of the $\cos^{2s}(\theta/2)$ model and the corresponding values of σ_θ plus and minus one standard deviation as a function of wave age β and suggestions from the literature.

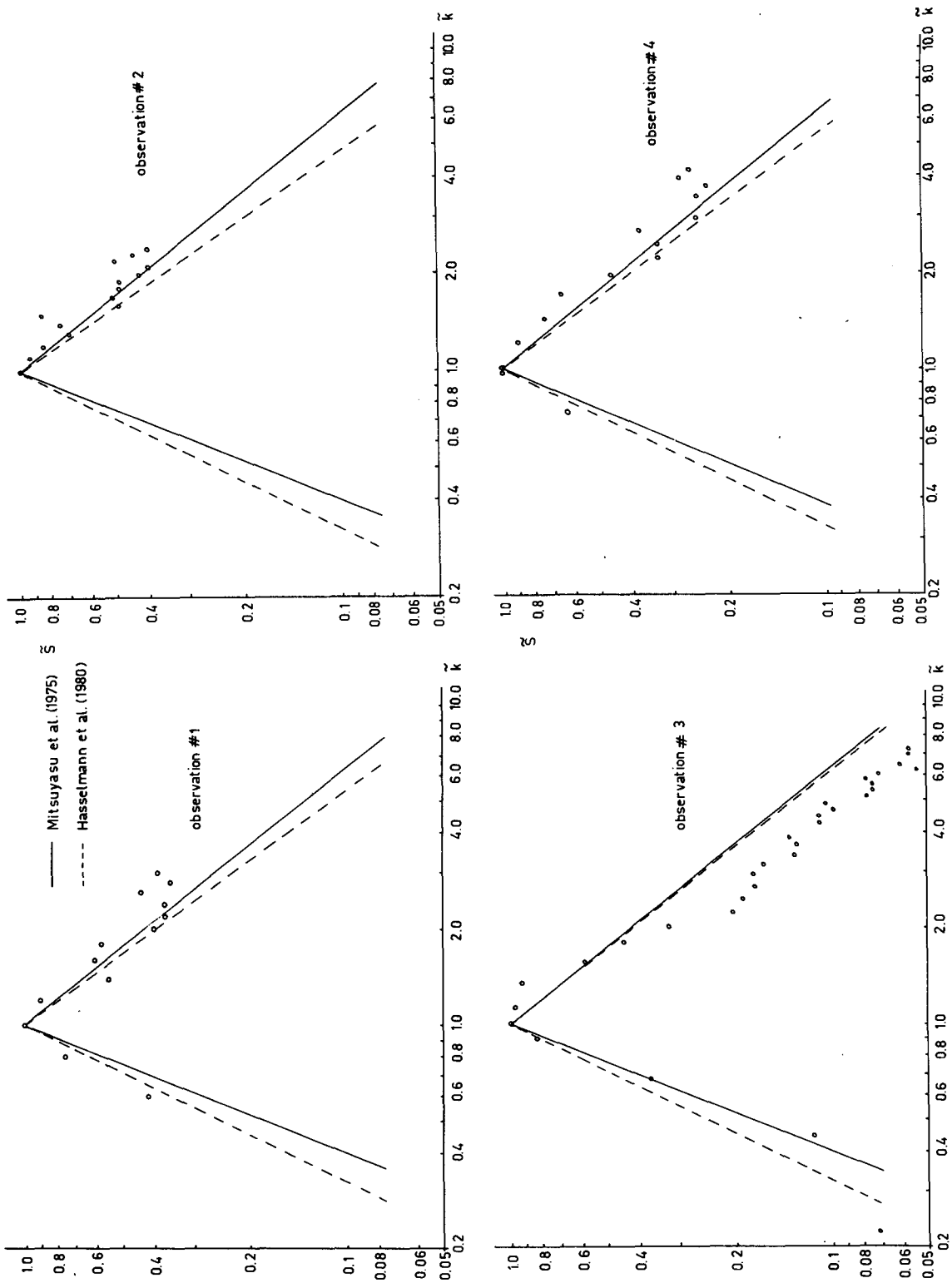

FIG. 17. The observed relative widening for observations 1–4 of the directional energy distribution from the peak of the spectrum to higher and lower wavenumbers quantified by the normalized directional width $\tilde{s}$ ($=s/s_m$) as a function of the normalized wavenumber $\tilde{k}$ ($=k/k_m$) and suggestions from the literature.

here in terms of frequencies, as in the original form, but in terms of wavenumbers. The transformation is based on the linear dispersion relationship, also for the transformation from peak frequency (f_m) to peak wavenumber (k_m). The latter seems to be acceptable for narrow spectra which are considered here. In addition, it will be convenient to consider separately the scale of s, quantified with the value of s at the peak of the spectrum ($s = s_m$ at $k = k_m$) and the normalized value of s ($\tilde{s} = s/s_m$).

MITSUYASU *et al.* (1975)

$$\left.\begin{aligned} \tilde{s} &= \tilde{k}^{2.5}, \quad \text{for} \quad \tilde{k} < 1 \\ \tilde{s} &= \tilde{k}^{-1.25}, \quad \text{for} \quad \tilde{k} \geq 1 \end{aligned}\right\}, \tag{20}$$

with

$$s_m = 11.5\beta^{2.5}. \tag{21}$$

HASSELMANN *et al.* (1980)

$$\left.\begin{aligned} \tilde{s} &= \tilde{k}^{2.03}, \quad \text{for} \quad \tilde{k} < 1 \\ \tilde{s} &= \tilde{k}^{(-0.32-0.72\beta^{-1})}, \quad \text{for} \quad \tilde{k} \geq 1 \end{aligned}\right\}, \tag{22}$$

with

$$\left.\begin{aligned} s_m &= 6.97, \quad \text{for} \quad \tilde{k} < 1 \\ s_m &= 9.77, \quad \text{for} \quad \tilde{k} \geq 1 \end{aligned}\right\}, \tag{23}$$

where the wave age β is defined as the ratio of the phase velocity at the spectral peak over the wind speed ($\beta = c_m/U$).

The results of this study are compared with the above expressions in Figs. 16 and 17. The standard deviation of s_m, which is indicated in Fig. 16, varies in terms of a directional sector from 1° to 5°. These values were estimated from a set of values of s_m obtained by fitting the $\cos^{2s}(\theta/2)$ model to 25 sample spectra of the population used in the Monte-Carlo technique that was described earlier.

The value of s_m in observation 1 in the ideal situation agrees (Fig. 16) with the suggestion of Hasselmann *et al.* (1980) as does, surprisingly, the s_m value in the irregular-coast situation where the $\cos^{2s}(\theta/2)$ model did not fit the observations particularly well. In the two other observations, of which one was taken in the ideal situation and the other in the slanting-wind situation, the observed values of s_m do not agree with either suggestion. In particular, the spectrum in the slanting-wind situation is directionally much more narrow than that appropriate to the expressions for s_m. This seems to be largely due to the influence of the geometry of the upwind coastline.

The observations of the normalized width parameter $\tilde{s}$ as a function of the normalized wavenumber $\tilde{k}$ agree fairly well with the suggestions (Fig. 17), perhaps slightly better with the suggestions of Mitsuyasu *et al.* (1975) than with the suggestions of Hasselmann *et al.* (1980) except for the observation in the slanting-wind situation (observation 3). In this observation the relative directional widening with increasing wavenumber from the peak wavenumber is more rapid than according to either of the suggestions. This again may be related to the geometry of the upwind coastline.

8. Conclusions

The following conclusions can be drawn from the 74 observations of the directional energy distribution which were obtained in this study from stereo pictures of the sea surface.

- In the ideal fetch-limited situation the $\cos^{2s}(\theta/2)$ model fits the observations of the directional energy distribution as well as one may expect from a statistical point of view.
- In a situation with an irregular upwind coastline, the shape of the two-dimensional spectrum is strongly influenced by the geometry of this coastline, at least if the scale of irregularities is equal to or larger than the distance offshore of the point under consideration. The observed influence and the results of hindcasts suggest a directionally decoupled generation of wind waves.
- The observed relative widening of the directional energy distribution from the peak wavenumber (or peak frequency) to lower and higher wavenumbers (or frequencies) agrees fairly well with suggestions in the literature for the ideal fetch-limited situation and, surprisingly, also for the non-ideal fetch-limited situations.

Acknowledgments. This study was supported by the Rijkswaterstaat (Department of Public Works in the Netherlands) with funding and operational assistance. I am particularly grateful to the Survey Department of this organization where Mr. A. H. Polderman, Mr. N. F. M. Bergen-Henegouwen and Miss J. Kronenberg with her colleagues have given their expert contributions to this study. The Royal Netherlands Air Force supported the study with helicopters which were flown by the Search and Rescue team of Soesterberg airbase. The officers and men of this team have performed a magnificent job. Significant support, both in logistics and scientific background was received from the group of scientists in JONSWAP whose interest I found most stimulating. Colleagues at the Royal Netherlands Meteorological Institute and at the Institute of Applied Physics have been very helpful during the operations off the Dutch coast. I am very grateful to Mr. G. J. v. d. Vliet of the Delft University of Technology for the development and operation of the electronic equipment. To Dr. J. A. Battjes of the University I am greatly indebted for his constant review of the study and for his many valuable suggestions.

REFERENCES

Brümmer, B., D. Heinricy, L. Krügermeijer and D. Prümm, 1974: The large scale weather features over the North Sea during

the JONSWAP II Experiment. Berichte des Instituts für Radiometeorologie und Maritime Meteorologie, Universität Hamburg, Institut der Frauenhofer Gesellschaft, No. 24, 55 pp.

Coté, L. J., J. O. Davis, W. Marks, R. J. McGough, E. Mehr, W. J. Pierson, J. F. Ropek, G. Stephenson and R. C. Vetter, 1960: The directional spectrum of a wind-generated sea as determined from data obtained by the Stereo Wave Observation Project. *Meteor. Pap.*, **2**, No. 6, New York University, College of Engineering.

Cruset, J., 1952: Photogrammetric measurements of the sea swell. *Photogrammetria*, 122–125.

Fox, M. J. H., 1976: On the nonlinear transfer of energy in the peak of a gravity-wave spectrum II. *Proc. Roy. Soc. London*, **A348**, 467–483.

Günther, H., W. Rosenthal, T. J. Weare, B. A. Worthington, K. Hasselmann and J. A. Ewing, 1979: A hybrid parametrical wave prediction model. *J. Phys. Oceanogr.*, **9**, 5727–5738.

Hasselmann, D. E., M. Dunckel and J. A. Ewing, 1980: Directional wave spectra observed during JONSWAP 1973. *J. Phys. Oceanogr.*, **10**, 1264–1280.

Hasselmann, K., R. P. Barnett, E. Bouws, H. Carlsen, D. E. Cartwright, K. Enke, J. A. Ewing, H. Gienapp, D. E. Hasselmann, P. Kruseman, A. Meerbrug, P. Müller, D. J. Olbers, K. Richter, W. Sell and H. Walden, 1973: Measurements of wind-wave growth and swell decay during the Joint North Sea Wave Project (JONSWAP). *Dtsch. Hydrogr. Z.*, **A8**, No. 12.

——, D. B. Ross, P. Müller and W. Sell, 1976: A parametric wave prediction model. *J. Phys. Oceanogr.*, **6**, 200–228.

Holthuijsen, L. H., 1981: The directional energy distribution of wind generated waves as inferred from stereophotographic observations of the sea surface. *Commun. Hydraul.*, Rep. No. 81-2, Dept. Civ. Eng., Delft University of Technology.

Jenkins, G. M., and D. G. Watts, 1968: *Spectral Analysis and its Applications*. Holden-Day, 525 pp.

Longuet-Higgins, M. S., D. E. Cartwright and N. D. Smith, 1963: Observations of the directional spectrum of sea waves using the motion of a floating buoy. *Ocean Wave Spectra*, Prentice Hall, 111–136.

Mitsuyasu, H., F. Tasai, T. Suhara, S. Mizuno, M. Ohkusu, T. Honda and K. Rikiishi, 1975: Observations of the directional spectrum of ocean waves using a cloverleafbuoy. *J. Phys. Oceanogr.*, **5**, 750–760.

Pierson, W. J., G. Neumann and R. W. James, 1955: Practical methods for observing and forecasting ocean waves by means of wave spectra and statistics. U.S. Navy Hydrographic Office, Publ. No. 603 (reprinted 1960).

Schumacher, A., 1939: Stereophotogrammetrische Wellenaufnahmen. *Wiss. Ergeb. Dtsch. Atlant. Exped. Forschungs Vermessung. "Meteor"* 1925–1927, Ozeanographische Sonderuntersuchungen, Erste Lieferung, Berlin.

Seymour, R. J., 1977: Estimating wave generation on restricted fetches. *Proc. ASCE, J. Waterway, Port, Coastal Ocean Div.*, **103**, No. WW2, 251–264.

Simpson, L. S., 1967: Preliminary investigation of the directional spectrum of ocean wave height as obtained from stereo wave photographs. Ocean Dynamics Branch, Exploratory Oceanography Division, Research and Development Department, U.S. Naval Oceanographic Office, Washington, DC, Informal Manuscript No. 67.1.

Singleton, R. C., 1969: An algorithm for computing the mixed radix fast Fourier transform. *IEEE Trans. Audio Electro-Acoustics*, **AU-17**, No. 2, 93–103.

Sugimori, Y., 1975: A study of the application of the holographic method to the determination of the directional spectrum of ocean waves. *Deep-Sea Res.*, **22**, 339–350.

Tyler, G. L., C. G. Teague, R. H. Stewart, A. M. Peterson, W. H. Munk and J. W. Joy, 1974: Wave directional spectra from synthetic aperture observations of radio scatter. *Deep-Sea Res.*, **21**, 989–1016.

Vliet, G. J. v. d., 1972: Stereofotografie van Zeegolven (Stereophotography of Sea Waves). Rep. No. 720013, Central Electronic Service Dept., Delft University of Technology.

——, 1974: Stereofotografie van Zeegolven 2 (Stereophotography of Sea Waves 2). Rep. No. 740022, Central Electronic Service Dept., Delft University of Technology.